NASA Technical Memorandum 89148

PLUME DISPERSION OF THE EXHAUST
FROM A CRYOGENIC WIND TUNNEL

WILLIAM S. LASSITER

JUNE 1987

NASA

National Aeronautics and
Space Administration

Langley Research Center
Hampton, Virginia 23665-5225

PLUME DISPERSION OF THE EXHAUST FROM A CRYOGENIC WIND TUNNEL

SUMMARY

An analytical model was developed to predict the behavior of the plume exhausting from the National Transonic Facility, a cryogenic wind tunnel at NASA, Langley Research Center. The model consists of two stages: the first stage was analytically resolved by assuming a Gaussian distribution of the plume thermodynamic properties in the radial direction and numerically integrating the momentum and diffusion equations; the second stage describes the descent of the plume and is resolved by describing the crosswind displacements by vorticity and numerically integrating in the crosswind and downwind directions. Temperature, visibility, oxygen concentration, and flow characteristics of the plume are calculated for distances downwind of the stack exhaust. Predictions are compared with several photographic observations. The model predicts the centerline trajectory of the plume fairly accurately, but underpredicts the extent of fogging. Revisions of the diffusion coefficient are made to bring the model in better agreement with the observations. Comparisons of the visible vertical spreading of the plume are made with Gaussian plume spreading.

SYMBOLS

A   empirical stability factor ($A = -3$ from ref. 3)

$\bar{a}$ mean droplet diameter (microns)

b   radius from exhaust jet axis to plume edge (m)

c   constituent concentration (kg/m^3)

c_p specific heat of air at constant pressure (cal/g-°K)

D   variable representing pressure, temperature, constituent concentration, water vapor content, or total water content of the exhaust

F   property of the exhaust

g   acceleration of gravity (9.8 m/sec^2)

k_o Von Karman universal constant ($k_o = 0.4$)

K	eddy diffusivity (m^2/sec)
K_{ref}	eddy diffusivity just above ground (0.15 cm^2/sec)
ℓ	turbulent eddy mixing length (m)
L	latent heat of condensation (cal/g)
Q_L	mass of liquid water per unit mass of air (kg/kg)
Q_T	total water mass (liquid + vapor) per unit mass of air (kg/kg)
r	radius from exhaust jet axis (m)
R	Richardson number
t	time (sec)
Δt	time increment (sec)
T	temperature (°K)
u	horizontal component of exhaust velocity in Stage I (m/sec)
U	horizontal wind speed (m/sec)
U_a	horizontal wind speed at 200 m altitude (m/sec)
v	plume horizontal component of velocity in crosswind (perpendicular to downwind direction x) plane (m/sec)
w	plume vertical component of velocity (m/sec)
x	distance downwind of stack (m)
Δx	increment of distance downwind of stack (m)
y	horizontal distance in the crosswind (perpendicular to downwind direction x) plane (m)
z	vertical distance (m)
z_o	surface roughness parameter (m)
α	entrainment coefficient
γ	atmospheric lapse rate (°K/km)
Γ	dry adiabatic atmospheric lapse rate (9.8°K/km)
∇^2	Laplacian operator (m^{-2})
θ	potential temperature in exhaust (°K)

λ	height at which eddy mixing length levels off (m)
ϕ	stream function (m^2/sec)
ξ	vorticity (sec^{-1})
ρ	density (kg/m^3)
ρ_w	density of water (g/cm^3)
σ	standard deviation of exhaust jet Gaussian distribution (m)

Subscripts

atm	atmospheric conditions
A	exhaust jet axis
e	at stack exit
ex	exhaust
m	mean
sat	saturation
*	ambient atmospheric conditions
I	first stage of plume
II	second stage of plume
1	point on jet vertical axis
2	point on jet vertical axis higher than point 1

INTRODUCTION

The literature contains many analytical and experimental studies of buoyant plumes, but few investigations into the behavior of negatively buoyant plumes. The purpose of this paper is to describe an analytical dispersion model and compare predictions of the model with observations of fogging from the negatively buoyant plume exhausting from the National Transonic Facility (NTF) (ref. 1). The NTF is a cryogenic wind tunnel used for testing advanced transport, fighter, and other aerospace models up to Reynolds numbers of 120 million at Mach 1 (fig. 1). Test section Mach numbers vary from 0.2 to 1.2. The tunnel, which achieves the high Reynolds

3

numbers by a combination of high pressure and low temperature, was designed to operate over temperatures from 77°K (-320°F) to 339°K (151°F) and pressures from atmospheric to 8.97 × 10^5 N/m^2 (130 psia) (ref. 1). Low temperatures are achieved by injecting liquid nitrogen (LN$_2$) through small nozzles positioned in the wind tunnel circuit upstream of the drive fan. The liquid, upon being sprayed into the tunnel, is vaporized and the cold nitrogen gas is accelerated as the test gas. Figure 2 is a schematic of the wind tunnel circuit, showing locations of LN$_2$ injection, the drive fan, and other components. Heat of compression from the fan vaporizes the liquid nitrogen. In order to establish steady thermodynamic conditions within the tunnel for testing, cold nitrogen gas is exhausted from the tunnel at the same mass flow rate as that of the LN$_2$ that is continuously injected. The inlet and exhaust systems were designed for up to 426 kg/sec (940 lb/sec) of nitrogen flow during normal operation (ref. 2).

The NTF exhaust system consists of special piping with relief valves, exhaust control (throttling) valves, and a fan/ejector system which mixes the cold exhaust gas with sufficient amounts of air for safe emission into the atmosphere (fig. 3), (ref. 2). An analytical computer program was devised which computes exhaust flow characteristics from the exit of the tunnel to the vent stack exit. The program calculates the mixing ratio of mass of air to mass of nitrogen by predicting the secondary air ingested by the nitrogen stream. Fan air from four 48-inch axial vane fans positioned at the base of the stack system was also taken into account. An operational map of air-to-nitrogen mixing ratio in the stack versus tunnel nitrogen exhaust gas (GN$_2$) flow is shown in figure 4 over the temperature range of operation. The fan/ejector system was designed such that the ejector produced an air-to-nitrogen mixing ratio at all times greater than one as the mixture exits the vent stack.

DESCRIPTION OF DISPERSION MODEL

The dispersion model begins at the top of the eleven foot diameter, 120-foot high NTF vent stack (see fig. 1). Secondary air flow rate, computed by the aforementioned exhaust system computer program and mapped in figure 4, and the nitrogen exhaust flow rate and temperature are inputs to the dispersion model. The model consists of two stages. The first stage describes the plume during ascent. The second stage begins when the vertical velocity is zero and describes the plume from then until completely mixed with the atmosphere. The second stage includes descent if the plume is negatively buoyant at the beginning of that stage.

Stage I

The first stage of the dispersion model is based on a vertical subsonic plume assumed to be steady state in the radial direction with properties expressed by the Gaussian relationship,

$$D = D_A \exp(-r^2/2\sigma^2) \tag{1}$$

where D is pressure, temperature, constituent concentration, water vapor content, or total water content. A momentum balance in the vertical direction at a point on the plume axis, considering buoyancy and diffusion, yields

$$\frac{dw}{dt} = g\left(\frac{\theta - \theta_*}{\theta_*}\right) + K(\nabla^2 w)_A \tag{2}$$

In the horizontal direction, the momentum balance yields,

$$\frac{du}{dt} = 2K \frac{\partial^2}{\partial r^2} (u_* - u) \tag{3}$$

From the diffusion equation,

5

$$\frac{d\theta}{dt} = 2K \frac{\partial^2}{\partial r^2}(\theta_* - \theta) + \frac{L}{c_p}\overline{\left(\frac{dQ_L}{dt}\right)}_{sat} \tag{4}$$

$$\frac{dc}{dt} = 2K \frac{\partial^2}{\partial r^2}(c_* - c) \tag{5}$$

$$\frac{dQ_T}{dt} = 2K \frac{\partial^2}{\partial r^2}(Q_{T*} - Q_T) \tag{6}$$

$$\frac{dQ_L}{dt} = 2K \frac{\partial^2}{\partial r^2}(Q_{L*} - Q_L) + \overline{\left(\frac{dQ_L}{dt}\right)}_{sat} \tag{7}$$

where $(dQ_L/dt)_{sat}$ is the change of liquid water due to evaporation if the vapor is unsaturated, or condensation if the vapor exceeds saturation. Once K and σ are defined, equations (1) through (7) are numerically integrated to determine the properties within the plume at any time.

The growth of σ with height z, (say from z_1 to z_2), was assumed to occur by deformation and diffusion, and is

$$\sigma_2^2 = \sigma_1^2 \frac{w_1}{w_2} + 2K_{ex}\left[\frac{z_2 - z_1}{\frac{1}{2}(w_1 + w_2)}\right] \tag{8}$$

where the first term is due to deformation and the second to diffusion with an exhaust eddy diffusivity of K_{ex}. The deformation term was arrived at by assuming conservation of volume in a steady state process and the radius of the exhaust to contain the fraction of effluent within one σ from the axis. The diffusion term was obtained from assuming the diffusion to be Gaussian with a variance of $(K_{ex1} + K_{ex2})\Delta t$. From equation (8),

$$\frac{1}{w_m\sigma_2^2} \frac{d}{dz} w_m\sigma_2^2 = \frac{2K_{ex}}{w_m\sigma_2^2} \tag{9}$$

6

where w_m is the mean velocity $1/2(w_1 + w_2)$ from z_1 to z_2. Equation (9) is equivalent to the mass conservation expression for a Gaussian distribution model (ref. 3).

$$\frac{1}{b^2 w_m} \frac{d}{dz} \left(b^2 w_m \right) = \frac{2\alpha}{b} \tag{10}$$

where α is an entrainment coefficient and b is the actual radius to the plume edge. Comparing equations (9) and (10) and assuming that $b \sim \sigma$ yields

$$K_{ex} = \alpha \sigma_2 w_m \tag{11}$$

for the plume-induced eddy diffusivity at the stack exit. Estimation of α can be made from plume observations by using equation (2.9) of reference 3.

During plume ascent the total eddy diffusivity is assumed to be

$$K_I = K_{ref} + K_{atm} + (K_{ex} - K_{atm}) \frac{w_m}{w_e} \tag{12}$$

where K_{ref} is a reference atmospheric turbulent eddy diffusivity just above ground and K_{atm} is the atmospheric turbulent eddy diffusivity which depends on atmospheric stability and wind conditions. In the first stage, K_{atm} is assumed to vary only in the z direction according to equation (13). Equation (12) is constructed such that at the stack exit, K_{ex} is the dominating diffusivity, and at the end of the first stage $K_{ref} + K_{atm}$ is dominant. K_{atm} is specified (ref. 3) as,

$$K_{atm} = \ell^2 \frac{dU}{dz} (1 + AR) \quad \text{for} \quad R < 0 \tag{13}$$

$$K_{atm} = \ell^2 \frac{dU}{dz} (1 - AR)^{-1} \quad \text{for} \quad R > 0 \tag{14}$$

where

$$R = \left(\frac{g}{T_A}\right)\frac{\gamma - \Gamma}{\left(\frac{dU}{dz}\right)^2}$$

(15)

and is defined as the Richardson number. A is an empirical stability factor determined from velocity fluctuation data in the Earth's boundary layer. In the first stage, $U = U_{amb}$. The turbulent eddy mixing length is (ref. 3),

$$\ell = \frac{k_o(z + z_o)}{1 + k_o\left(\frac{z + z_o}{\lambda}\right)}$$

(16)

where $\lambda = 2.7\ U_a$ (ref. 4) and U_a is a constant wind speed that U_{amb} approaches at an altitude of 200 m. Equation (13) is used for a stable atmosphere and equation (14) for an unstable atmosphere.

Stage II

The second stage of the dispersion model begins once the vertical velocity decreases to zero. The plume is assumed to drift downwind with the horizontal wind speed (x direction) and displacements in the plane perpendicular to the downwind x direction (crosswind) are described by the vorticity,

$$\xi = \frac{dw}{dy} - \frac{dv}{dz}$$

(17)

The properties C, Q_T, Q_L, θ, and ξ in the crosswind plane are expressed through the diffusion equation as

$$\frac{dc}{dt} = \frac{\partial}{\partial z}\ K\ \frac{\partial c}{\partial z} + \frac{\partial}{\partial y}\ K\ \frac{\partial c}{\partial y}$$

(18)

$$\frac{dQ_T}{dt} = \frac{\partial}{\partial z}\ K\ \frac{\partial Q_T}{\partial z} + \frac{\partial}{\partial y}\ K\ \frac{\partial Q_T}{\partial y}$$

(19)

8

$$\frac{dQ_L}{dt} = \frac{\partial}{\partial z} K \frac{\partial Q_L}{\partial z} + \frac{\partial}{\partial y} K \frac{\partial Q_L}{\partial y} + \left(\frac{dQ_L}{dt}\right)_{sat} \tag{20}$$

$$\frac{d\theta}{dt} = \frac{\partial}{\partial z} K \frac{\partial\theta}{\partial z} + \frac{\partial}{\partial y} K \frac{\partial\theta}{\partial y} + \frac{L}{c_p}\left(\frac{dQ_L}{dt}\right)_{sat} \tag{21}$$

$$\frac{d\xi}{dt} = \frac{\partial}{\partial z} K \frac{\partial\xi}{\partial z} + \frac{\partial}{\partial y} K \frac{\partial\xi}{\partial y} + \frac{\partial}{\partial y}\left(g \frac{\theta}{\theta_*}\right) \tag{22}$$

where the last term in equation (22) is the torque due to the horizontal gradient of buoyancy. The initial vertical motion in the second stage is generated by this torque and the changes in properties over a downwind distance Δx are computed using the operator,

$$\Delta F = \frac{\partial F}{\partial x} \Delta x = \left(\frac{\Delta x}{U}\right)\left(\frac{dF}{dt} - v \frac{\partial F}{\partial y} - w \frac{\partial F}{\partial z}\right) \tag{23}$$

where F is either of the properties C, Q_L, Q_T, θ or ξ. After obtaining ξ at the downwind distance $x + \Delta x$, a field or stream function ϕ is derived satisfying,

$$\nabla^2\phi = \xi = \frac{\partial w}{\partial y} - \frac{\partial v}{\partial z} \tag{24}$$

where

$$w = \frac{\partial\phi}{\partial y} \tag{25}$$

and

$$v = -\frac{\partial\phi}{\partial z} \tag{26}$$

from which w and v are determined at the new distance $x + \Delta x$. The eddy diffusivity K for the second stage used in equations (18)-(22) is

$$K_{II} = K_{ref} + K_{atm} \tag{27}$$

where, in the second stage, U in equations (13), (14), and (15) is composed of
the y and z direction velocities, v and w, respectively.

Visibility is calculated by the equation

$$V = 2.61 \; \rho w \; \frac{\bar{a}}{Q_L} \qquad\qquad (28)$$

(ref. 5) in both stages of the plume dispersion model. In the first stage, visibil-
ity on the plume centerline as a function of altitude is calculated. In the second
stage, visibility is calculated as a function of y and z in the crosswind plane
and as a function of downwind distance x.

COMPARISON OF PLUME PHOTOGRAPHS WITH ANALYTICAL PREDICTIONS

The plume from the NTF vent stack was observed and photographed during several
tunnel runs occurring on different days at different atmospheric conditions. A
balloon carrying an instrument package for measuring wind speed and direction, rela-
tive humidity, temperature, and pressure was launched within 1-2 hours prior to or
during each run. The package consisted of a three cup anemometer for wind speed
measurement; an electrical clamping compass using the balloon as a wind vane for wind
direction measurement; a wet-dry bulb aspirator using thermistors for humidity and
temperature measurement; and a transducer for pressure measurement. Data were
telemetered to a receiver on the ground and recorded real time. The balloon was
launched to an altitude of about 500 feet, which was higher than plume ascent.
Figure 5 is a photograph of the balloon. The wind and temperature profiles as a
function of altitude, and the pressure and relative humidity at the maximum plume
height were inputs to the plume dispersion model. Estimated mass flows of nitrogen
and secondary air pumped by the vent stack ejector were also inputs to the dispersion
model. The nitrogen exhaust flow rate was estimated by thermodynamic computations
using tunnel pressure, temperature, and drive motor horsepower. The ejector

secondary air flow rate was estimated using the earlier mentioned exhaust flow analytical model developed at LaRC based on previously developed engineering practice (ref. 6).

Figures 6, 7, and 8 are photographs of the plume during tunnel nitrogen exhaust flows of 193.2 kg/sec (426 lb/sec), 298 kg/sec (657 lb/sec), and 345.1 kg/sec (761 lb/sec), respectively. Vent stack exit temperatures of these three runs were calculated to be 239.2°K (-28.8°F), 229.1°K (-47.1°F), and 223.1°K (-56.4°F). Measured atmospheric surface wind speed, relative humidity, and temperature were 5.5 m/sec (12.3 mph), 74 percent, and 294.1°K (70°F), respectively. The measured atmospheric lapse rate was (-12.3°K/km) (-.0053°F/ft). The dark line indicates the prediction by the dispersion model of the plume centerline and the distance downwind at which the fog dissipates. Prediction of the centerline appears to agree well with the observations, but the model predicted fog dissipation at a less distance downwind than observed. Note that the plume dissipates before reaching stage II (maximum height).

Observations were made of the plume at a later date at a relative humidity of 94 percent, ambient temperature of 281.9°K (48°F), and a surface wind speed of 2.68 m/sec (6 mph). The high humidity resulted in significant fogging in the second stage of the plume. Table 1 shows a summary of these observations. Three observations were made at a nitrogen mass flow of 270.7 kg/sec (597 lb/sec). The means of the maximum plume centerline heights, distances downwind at which these maximum heights occurred, and the plume widths at the maximum heights are shown in table 1, along with the analytical model predictions. Results of an observation at a nitrogen mass flow rate of 207.7 kg/sec (458 lb/sec) are also shown in table 1, along with the analytical model predictions. Predicted values of the centerline maximum height and plume width at that maximum height were within about 20 percent of observed values. Observed values of the distance downwind of this maximum height were not as much in agreement. Figure 9 shows a representative observation of one of the runs at

270.7 kg/sec, (597 lb/sec) nitrogen flow. The dark line is the centerline predicted

by the model. Figure 10 shows an observation at 207.7 kg/sec (458 lb/sec) of

nitrogen flow and the predicted centerline. The model agrees with the observations

in that it predicts descent of the plume due to negative buoyancy. The model,

though, predicts plume touchdown on the ground at a distance from the stack much

greater than observed. The observed fog descended to ground level, breaking up just

before touching ground. The model was revised somewhat, to obtain the agreement

shown in Figures 9 and 10. The K_{atm} was decreased by a factor of 200, which

generated more fog for further distances downwind. The entrainment coefficient α

was estimated to be about 0.15 by measuring the radial spread of the plume from

close-up photographs and using equation 2.9 of reference 2.

Predicted centerlines in Figures 9 and 10 agree fairly well with the observed

plume behavior. In both figures, the visible plume vertical widths increase in the

second stage with downwind distance. The model predicted in both cases a constant

vertical width for a distance downwind, then a slightly decreasing vertical width

with further increase in downwind distance. The observed vertical widths were deter-

mined by fairing-in plume boundaries from the photographs. Half widths were then

plotted and compared with the vertical spreading parameters, or standard deviations,

recommended by Briggs (ref. 7) for all stability classes and used in Gaussian plume

analyses. Comparison of these curves indicates the spreading of the visible plumes

to be in accordance with stability classes C or D, which are slightly stable or

neutral stability classes, respectively. The measured atmospheric lapse rate during

these observations was -9.83°K/km (-.0042°F/ft) which corresponds to a neutral

stability class. The difference in slopes of the boundaries between the observed

plume and the neutral stability class was estimated to be only 1-2 degrees. Some of

this difference could be accounted for by error in fairing the boundaries of the

observed plume. Thus, the observations imply that the fog produced in the cyrogenic

plume spreads in the vertical direction similarly to that of a Gaussian plume.

12

SOURCES OF ERROR

Several sources of error are possible which could contribute to differences in observations and predictions. The plume could be colder than predicted, which would account for the higher predicted height of the centerline. No measurements of plume properties were performed. Since neither mass flow rate of nitrogen nor that of secondary air were measured, either could be higher or lower than used in the predictions. This could significantly affect plume maximum height, temperature, and downwind trajectory. The diffusion of the plume in the atmosphere could be occurring at a different rate than expressed through the Richardson number. Measurements of temperature, exhaust velocity, air and nitrogen flowrates, and constituent concentrations inside the plume would give insight into the sources of error. Scaling dimensions of the plume from the photographs was a source of error. Attempts were made to locate the camera line of sight perpendicular to the downwind direction. No relative measurements of this location were made. The photographs were taken at ground distances from the plume of at least five times the plume height, in order to attempt to reduce errors in estimating the true vertical width of the plume. No adjustments of measurements were made for parallax.

CONCLUSIONS

A numerical disperison model of a cold jet dispersing in the atmosphere was devised for the NTF. Photographs of the exhaust plume on several rather humid (relative humidities >70%) days were made and compared with the plume trajectory and shape predicted by the plume dispersion model. Agreement between the model and observations is good for the centerline trajectory of the plume. The model predicts descent of the plume in stage II, due to negative buoyancy. The predicted descent of the plume, with downwind distance, is less than that observed. This could be attributable to lower temperatures in the plume than predicted, or errors in estimation of

the gaseous nitrogen flow rate, or the atmospheric air ingested by the exhaust system.

Diffusion terms in the model were decreased in the second (descent) stage in order to increase the predicted fog to be in better agreement with that observed. The model predicted a constant plume width in stage II for some distance downwind, then decreasing with further distance. The observed plume widths in stage II increased in accordance with slightly stable or neutral stability class spreading of a Gaussian plume. This implies that the negative buoyant plume was spreading in a vertical direction similarly to that of a Gaussian plume. The plume dispersion was sufficient for NTF operations. More observations are planned in the future to compare with predictions.

COMPUTER CODE

The computer code used to develop the predictions is being modified to alleviate spurious effects on temperature predictions at low wind speeds. These effects were not evident in the results presented herein, but were noticed when performing parametric studies. The effects appear to be computational in nature. Switching to a LaGrangian from an Eulerian approach to integrating in the plume second stage in the downwind direction appears to alleviate the spurious computational effects.

The computer code also contains many statements for experimental computational purposes which may be confusing to the reader without further explanation. These statements were included to aid in the development of the code and for debugging purposes. For the above reasons, the code is not attached to this publication. It is intended to use the modified LaGrangian code in comparing predictions with future observations at conditions different than presented herein. An attempt to cleanse the code of the extraneous statements will be made such that future publication may occur.

ACKNOWLEDGEMENTS

TABLE I.   SECOND STAGE PLUME DIMENSIONS

Observed vs. Predicted

	Observed	Predicted
Centerline maximum height, m	105.9* 119$^\Delta$ (mean)	116.7* 135$^\Delta$
Distance downwind of centerline at maximum height, m	59.7* 97.3$^\Delta$ (mean)	120.5* 148.8$^\Delta$
Width at centerline maximum height, m	55* 61.5$^\Delta$ (mean)	50* 50$^\Delta$

*207.7 kg/sec (458 lb/sec) Nitrogen Mass Flow Rate
$^\Delta$270.7 kg/sec (597 lb/sec) Nitrogen Mass Flow Rate

REFERENCES

1. Bruce, Walter E., Jr.; Fuller, Dennis E.; and William B. Igoe: National Transonic Facility Shakedown Test Results and Calibration Plans. Paper No. 84-0584CP. Presented at the AIAA 13th Aerodynamic Testing Conference, San Diego, CA, March 5-7, 1984.

2. Ivey, George W., Jr.: Cryogenic Gaseous Nitrogen Discharge System. NASA Conference Publication 2122, Part I, November 27-29, 1979, pp. 271-278.

3. Hoot, T. G.; Meroney, R. N.; and J. A. Peterka: Wind Tunnel Tests of Negatively Buoyant Plumes. Environmental Protection Agency Document EPA-650/3-74-003, October 1973.

4. Estoque, Mariano A.; and Chandrakant M. Bhumralkar: A Method for Solving the Planetary Boundary-Layer Equations. Boundary Layer Meteorology, Vol. 1, 1970, pp. 169-194.

5. Johnson, John C.: Physical Meteorology. John Wiley & Sons, New York, 1960.

6. Kastner, L. J., et. al.: An Investigation of the Performance and Design of the Air Ejector Employing Low-Pressure Air as the Driving Fluid. Institute of Mechanical Engineers Proceedings, Vol. 162, No. 2, 1950, pp. 149-166.

7. Hanna, Steven R.; Briggs, Gary A.; and Rayford P. Hosker, Jr.: Handbook on Atmospheric Diffusion. DOE/Tic-11223 Technical Information Center, U.S. Department of Energy, 1982.
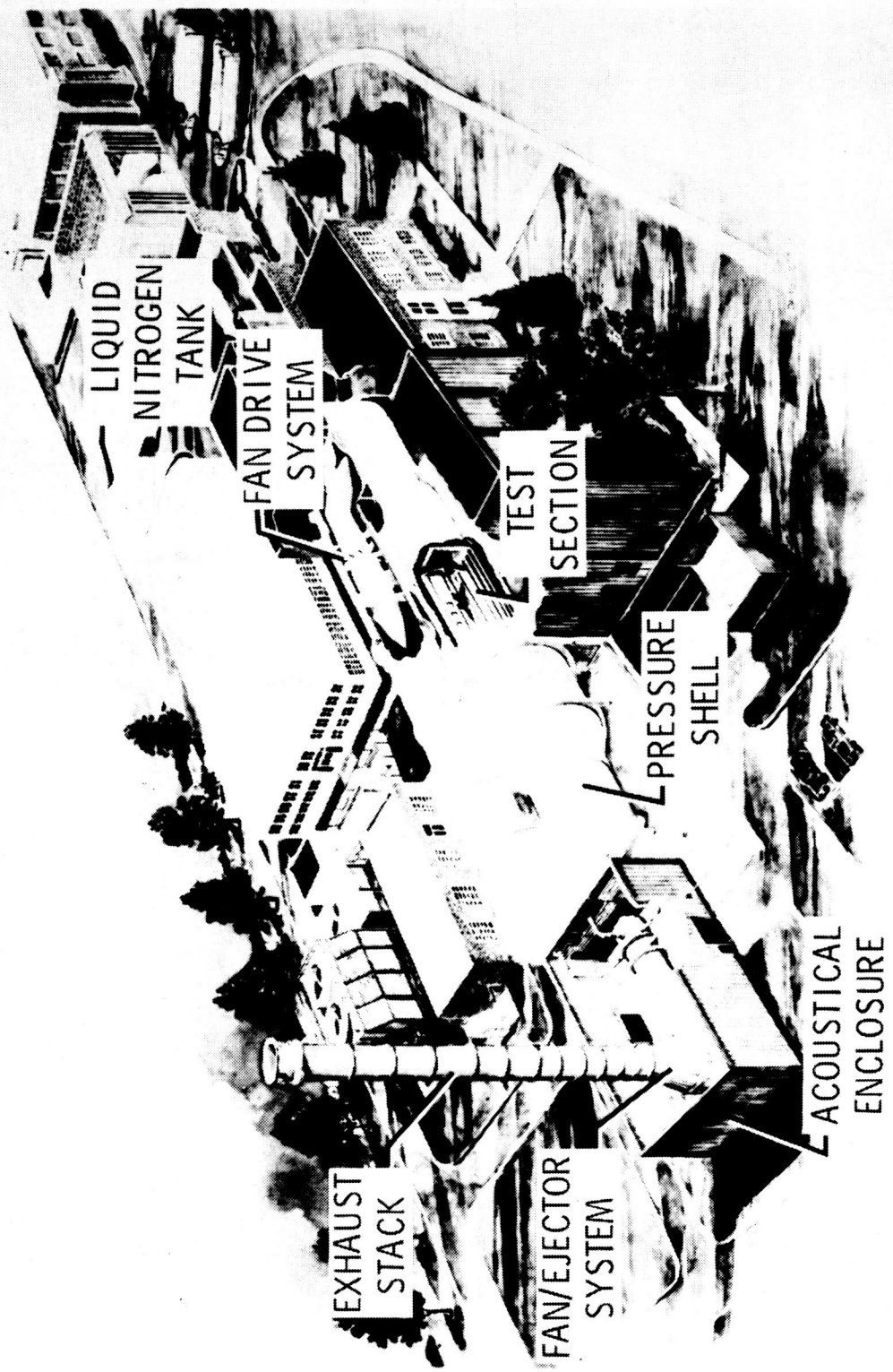
Figure 1. - Artist concept of NTF.

Labels in figure: LIQUID NITROGEN TANK, FAN DRIVE SYSTEM, TEST SECTION, PRESSURE SHELL, ACOUSTICAL ENCLOSURE, EXHAUST STACK, FAN/EJECTOR SYSTEM
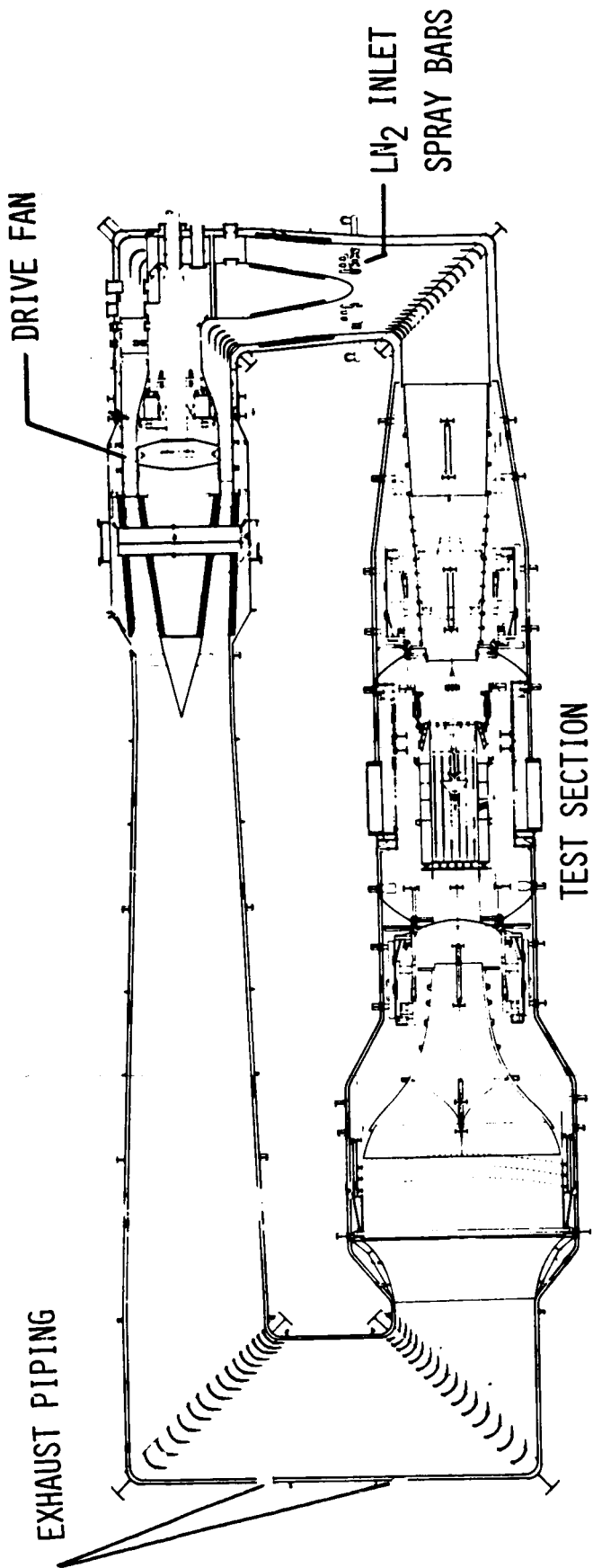
Figure 2. - Schematic of NTF circuit and location of LN₂ inlet and outlet.

DRIVE FAN

LN₂ INLET SPRAY BARS

TEST SECTION

EXHAUST PIPING

EXHAUST CONTROL VALVES

MUFFLER

ACOUSTICAL ENCLOSURE

DISCHARGE VESSEL

EXHAUST MIXTURE

STACK

MIXING PLANE

FAN/EJECTOR SYSTEM

SECONDARY AIR

FAN AIR
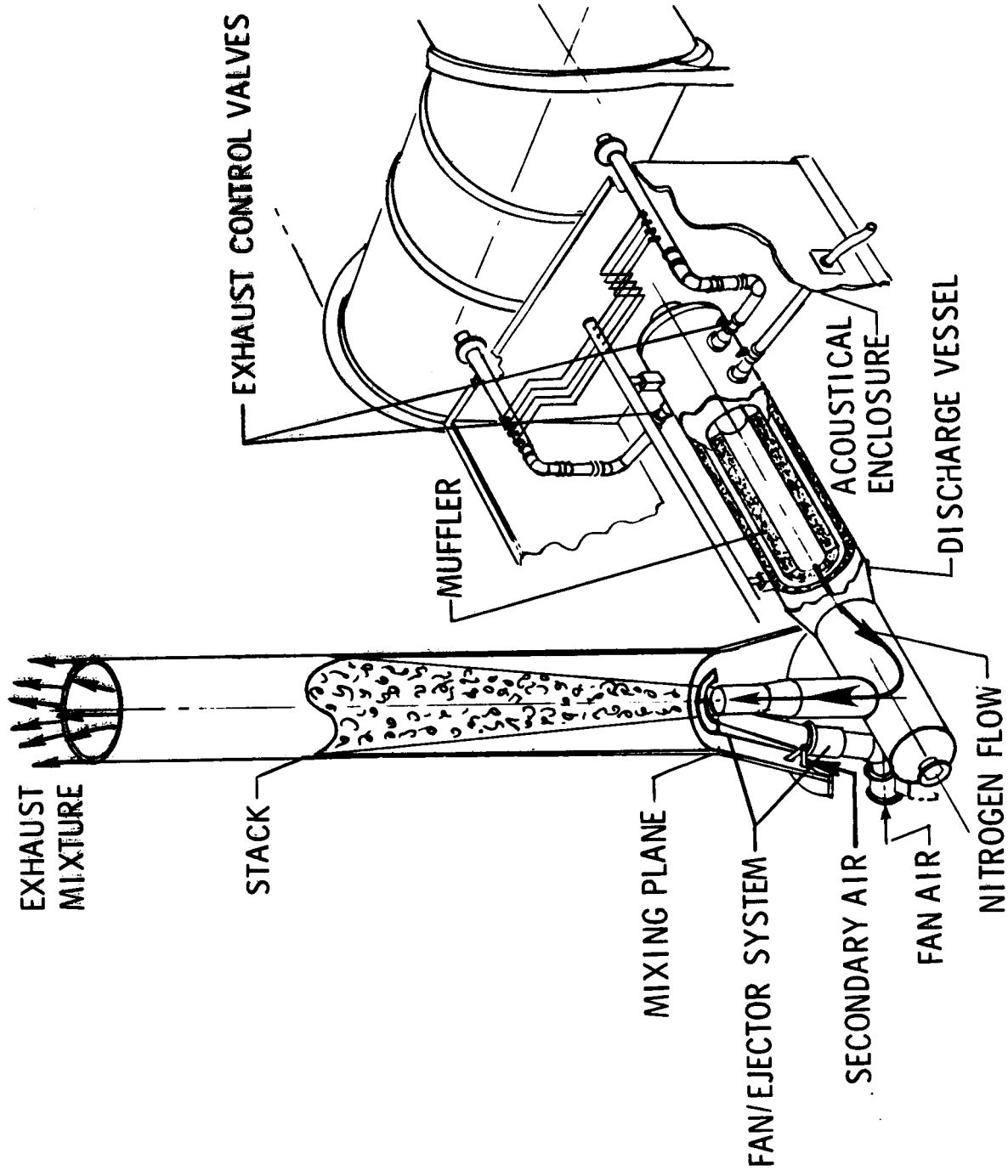
NITROGEN FLOW

Figure 3. - NTF exhaust system.
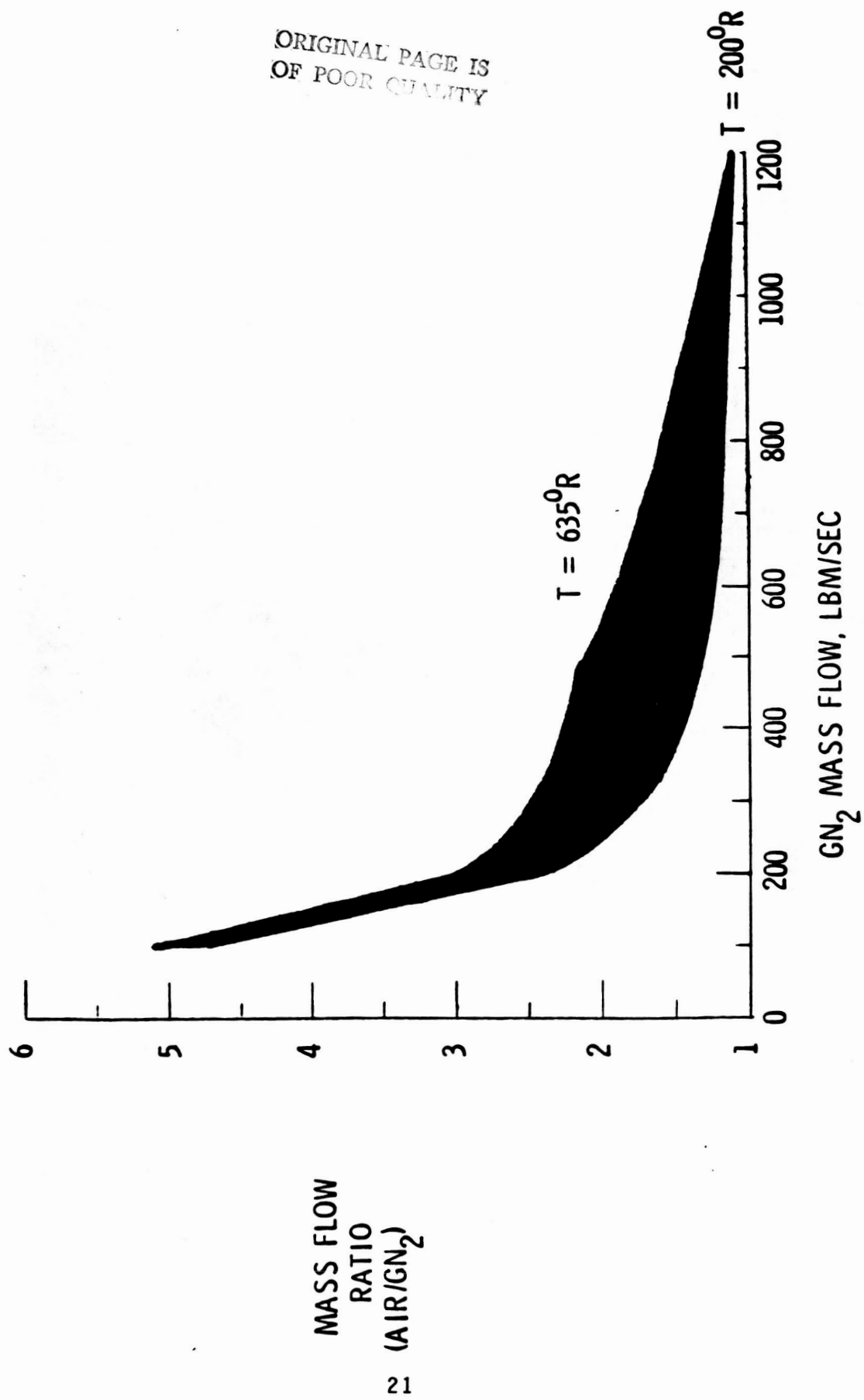
Figure 4. - NTF exhaust stack dilution of gaseous nitrogen.
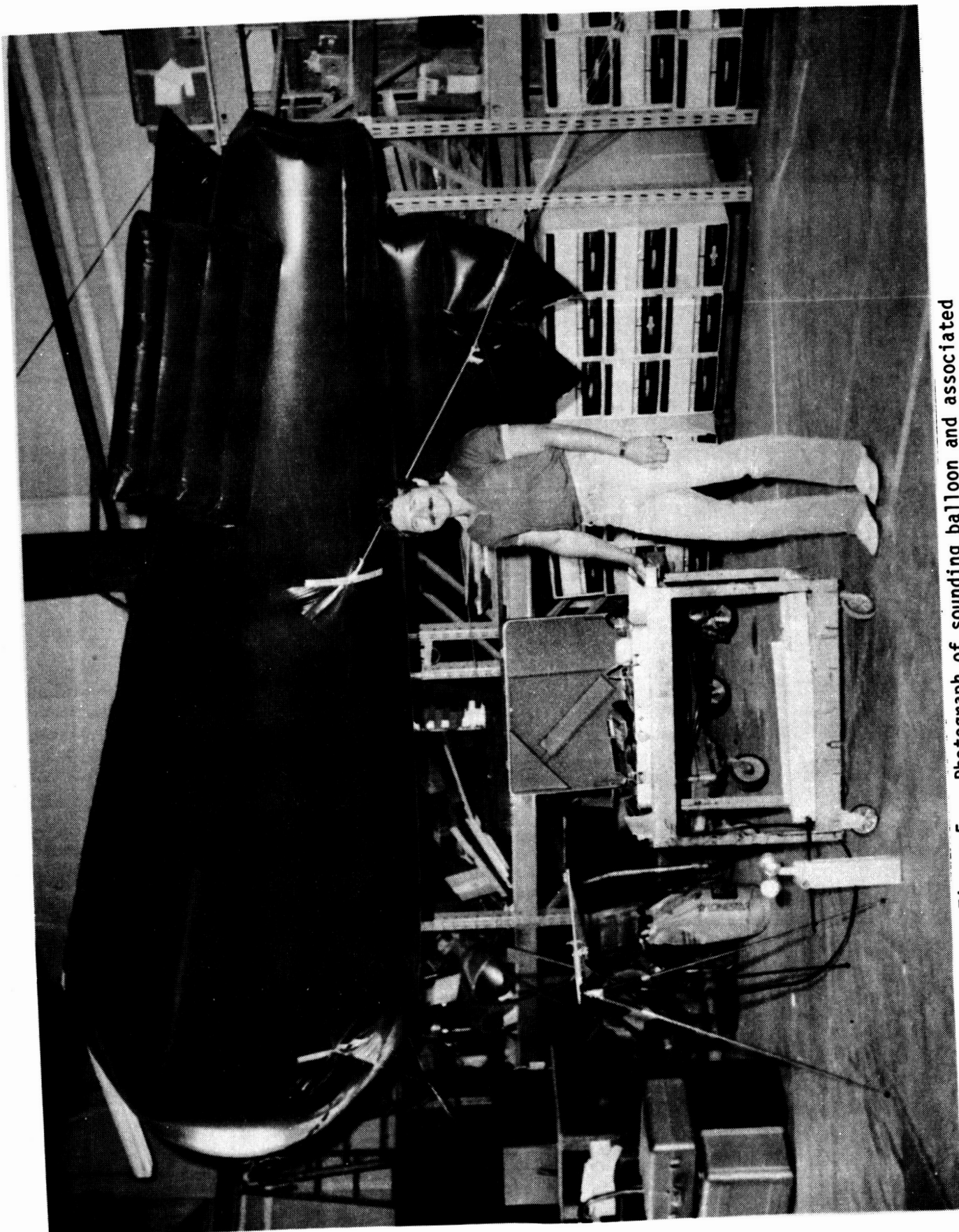
Figure 5. - Photograph of sounding balloon and associated instrumentation.

22
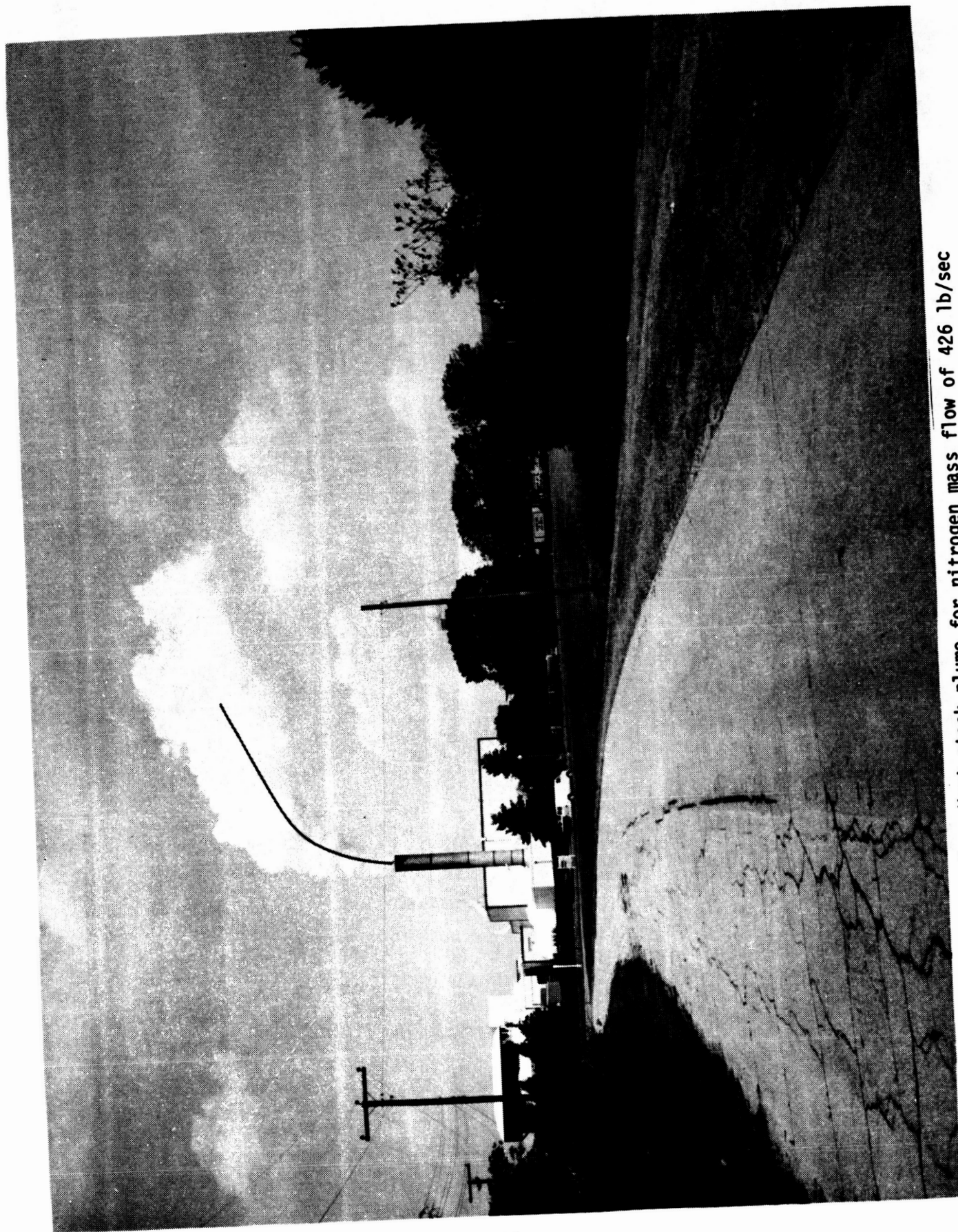
Figure 6. - Vent stack plume for nitrogen mass flow of 426 lb/sec and relative humidity of 74%.
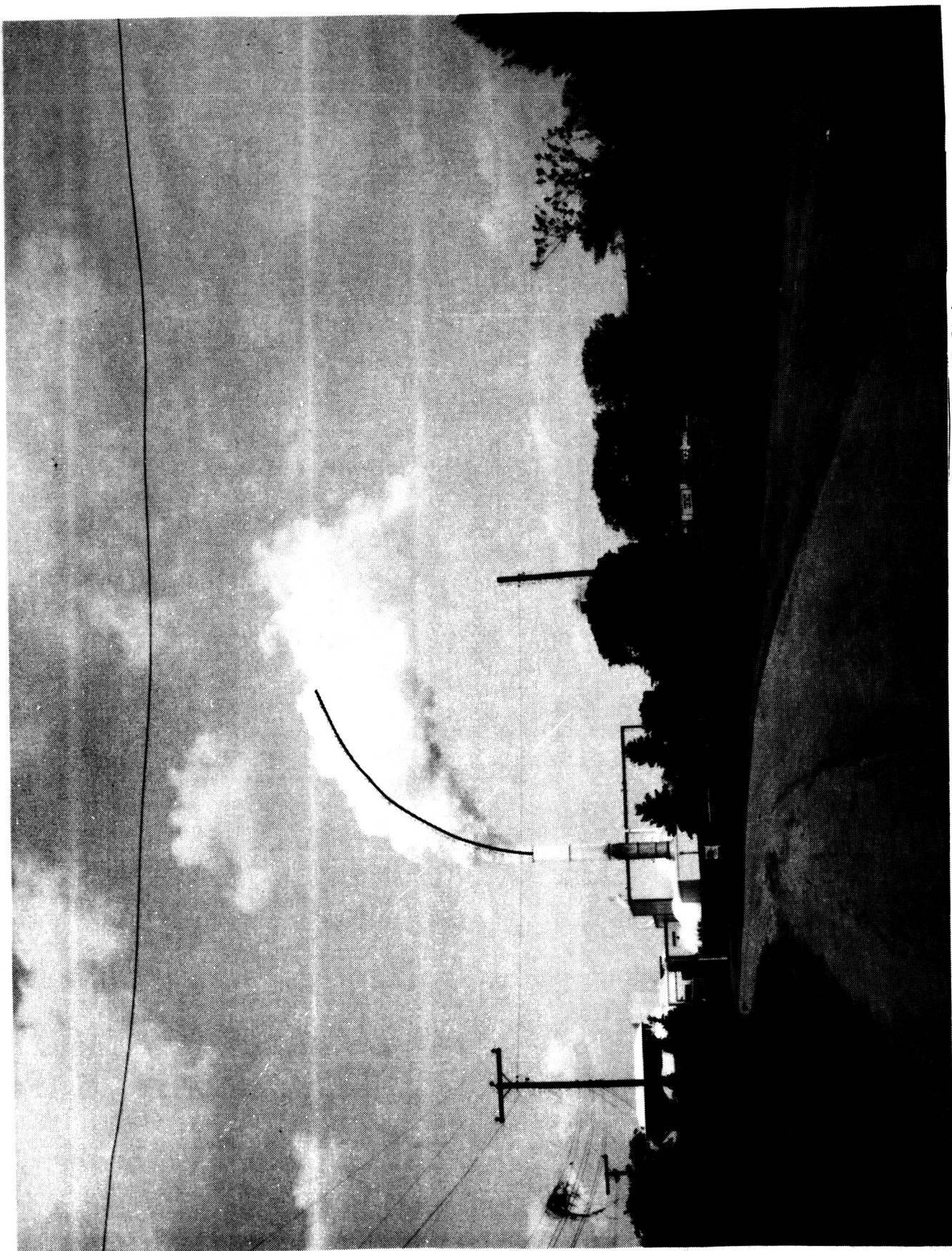
Figure 7. - Vent stack plume for nitrogen mass flow of 657 lb/sec and relative humidity of 74%.

24
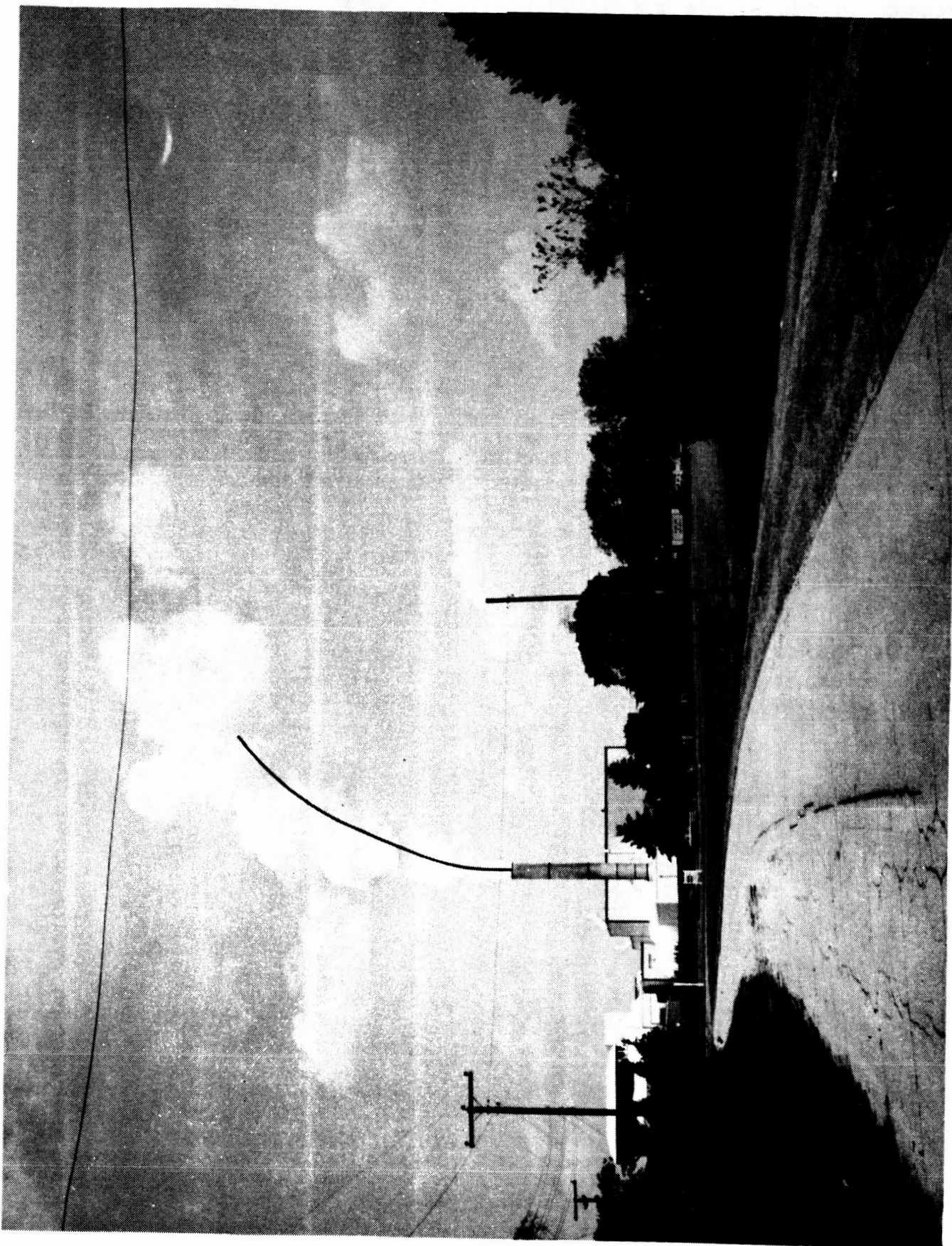
Figure 8. - Vent stack plume for nitrogen mass flow of 761 lb/sec and relative humidity of 74%.

25
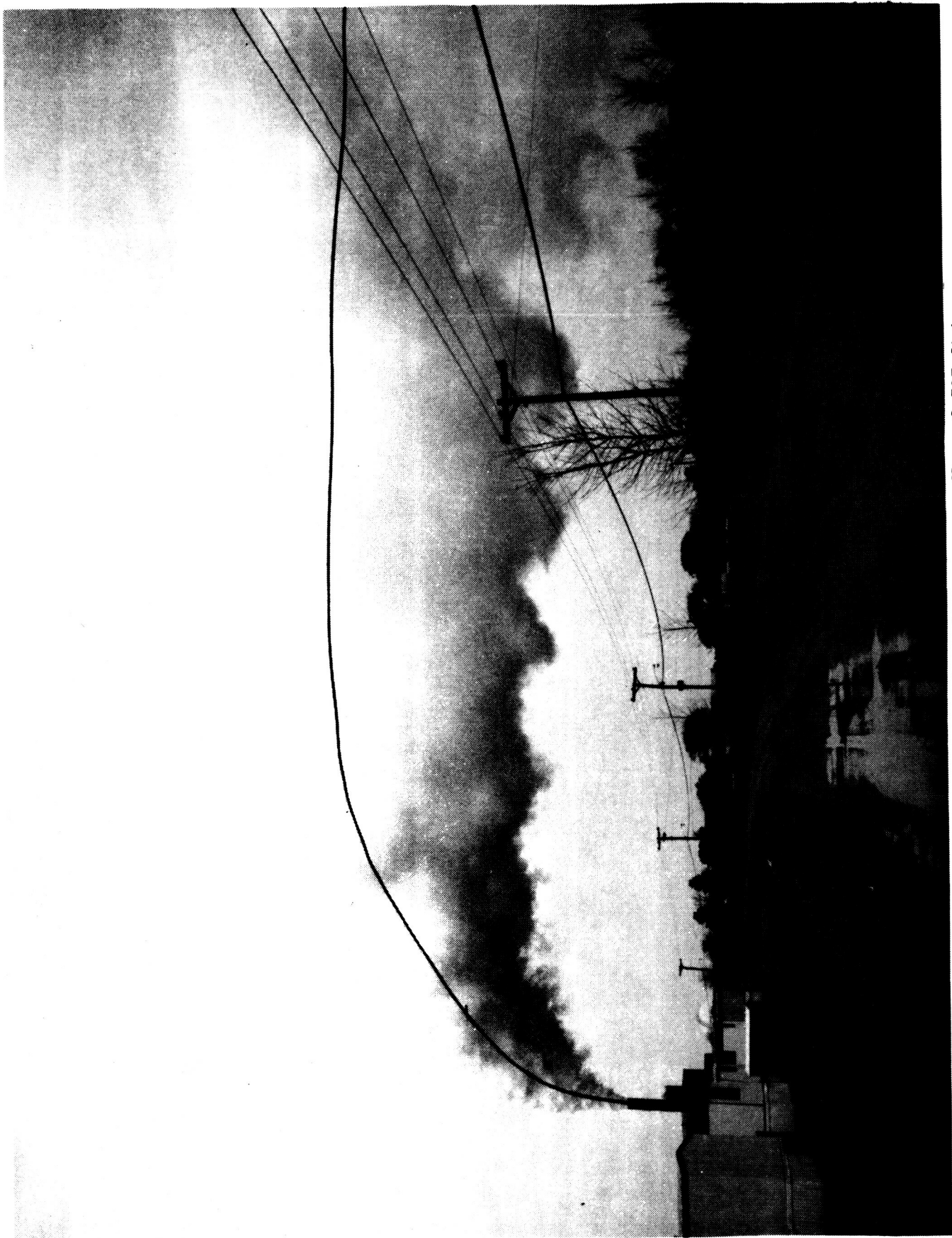
Figure 9. - Vent stack plume for nitrogen mass flow of 597 lb/sec and relative humidity of 94%.

26
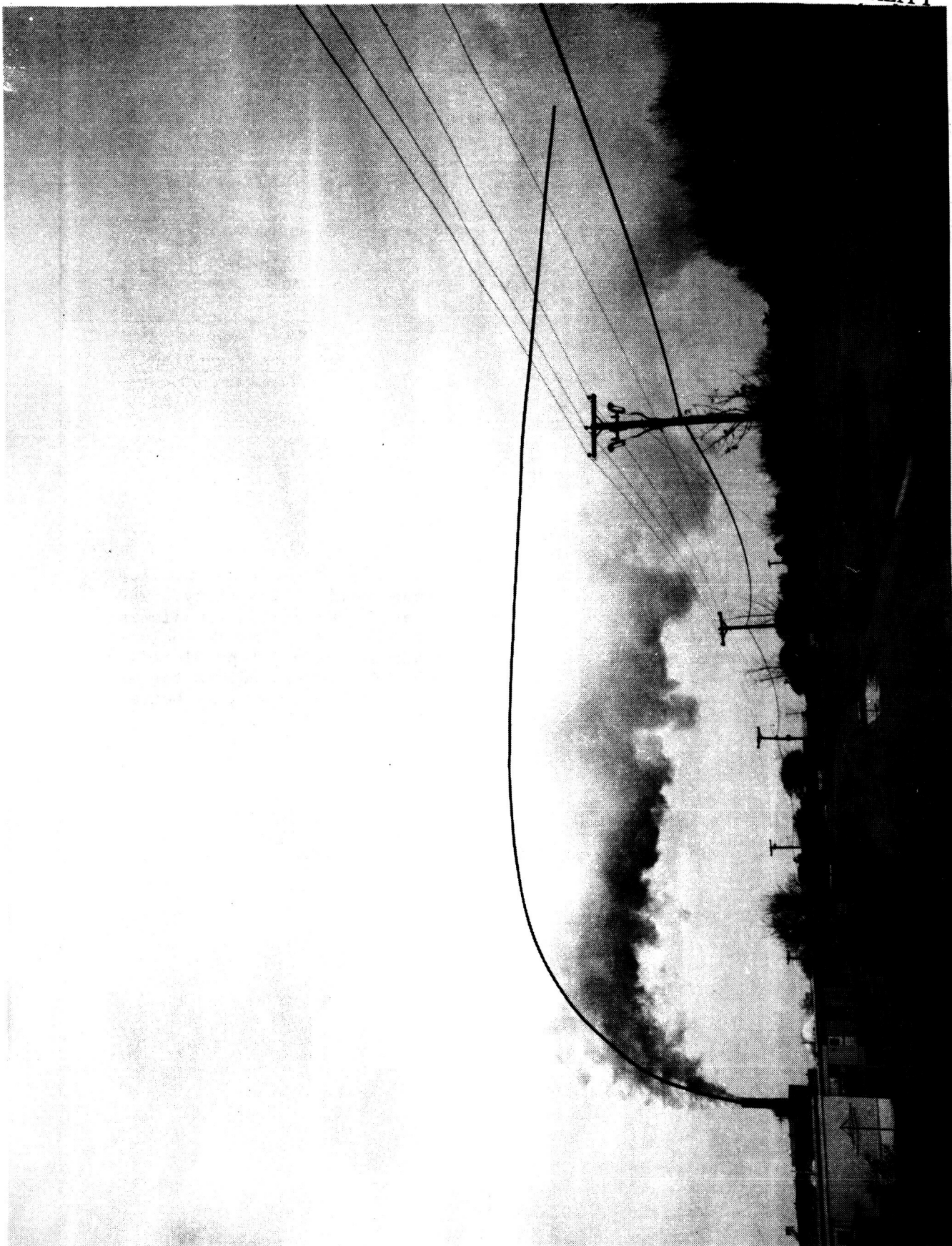
Figure 10. - Vent stack plume for nitrogen mass flow of 458 lb/sec and relative humidity of 94%.

27

Standard Bibliographic Page

1. Report No. NASA TM-89148	2. Government Accession No.	3. Recipient's Catalog No.
4. Title and Subtitle Plume Dispersion of the Exhaust from a Cryogenic Wind Tunnel		5. Report Date June 1987
		6. Performing Organization Code
7. Author(s) William S. Lassiter		8. Performing Organization Report No.
9. Performing Organization Name and Address NASA Langley Research Center Hampton, VA 23665-5225		10. Work Unit No. 505-61-01-01
		11. Contract or Grant No.
12. Sponsoring Agency Name and Address National Aeronautics and Space Administration Washington, D. C. 20546-0001		13. Type of Report and Period Covered Technical Memorandum
		14. Sponsoring Agency Code

15. Supplementary Notes

16. Abstract

An analytical model was developed to predict the behavior of the plume exhausting from the cryogenic National Transonic Facility. Temperature, visibility, oxygen concentration, and flow characteristics of the plume are calculated for distance downwind of the stack exhaust. Negative buoyancy of the cold plume is included in the analysis. Compared to photographic observations, the model predicts the centerline trajectory of the plume fairly accurately, but underpredicts the extent of fogging. The diffusion coefficient is revised to bring the model in better agreement with observations.

17. Key Words (Suggested by Authors(s)) Fluids, Plumes, Jets, Cryogenic Plumes	18. Distribution Statement Unclassified – Unlimited Subject Category 34		
19. Security Classif.(of this report) Unclassified	20. Security Classif.(of this page) Unclassified	21. No. of Pages 28	22. Price A03